Tuijin Jishu/Journal of Propulsion Technology
ISSN: 1001-4055
Vol. 47 No. 02 (2026)

Design, Analysis and Retrofitting of an Internal Combustion Engine Mini-Truck into an Electric Vehicle

Bharath S Krishnan[1], Nidhi M B[2], Chitrakumar V K[3]

[1,2] Department of mechanical Engineering, Mar Baselios College of Engineering and Technology (Autonomous), Trivandrum, India

[3] Department of Mechanical Engineering, Sree Chitra Thirunal College of Engineering, Trivandrum, India

Abstract: The growing concerns over vehicular emissions and rising fuel consumption have accelerated the need for sustainable transportation solutions. Electric vehicle (EV) retrofitting has emerged as a cost-effective and practical alternative to the adoption of new EVs, particularly for small commercial vehicles widely used in urban transport. This study focuses on the conversion of a conventional internal combustion engine (ICE)-based mini-truck into a fully electric vehicle. The power and torque requirements under various driving conditions, including acceleration, steady-state motion, and inclined travel, are evaluated using analytical and numerical approaches. Standard vehicle dynamics equations are employed for theoretical analysis, while MATLAB Simulink is utilized to simulate realistic drive cycles and obtain dynamic performance characteristics. Based on the obtained results, suitable motor and battery specifications are identified, leading to the selection of a Permanent Magnet Synchronous Motor (PMSM) due to its high efficiency and superior performance. Furthermore, key mechanical components such as the motor mounting clamp, mounting plate, coupler, and fastening system are designed and modelled using CAD tools. Structural analysis is conducted using ANSYS to assess stress distribution, strain, and deformation under operational loading conditions. The results demonstrate that all designed components are structurally reliable, exhibiting minimal deformation and stress values well within permissible material limits.The study validates the feasibility of EV retrofitting as an efficient and sustainable solution for reducing emissions in urban transportation.

Keywords: Retrofitting, Permanent Magnet Synchronous Motor (PMSM), ANSYS Structural Analysis, MATLAB Simulink Simulation

1. Introduction

Automobile-related pollution has increased rapidly, with nearly 74% of total emissions attributed to the use of internal combustion engines (ICEs) [1]. According to estimates by the United Nations Environment Programme (UNEP), the transport sector accounts for approximately 25% of global energy-related greenhouse gas emissions [2]. In response to growing environmental and economic concerns, electric vehicles (EVs) have recently gained greater prominence compared to conventional gasoline-powered vehicles [3]. EVs produce zero direct emissions and play a significant role in improving urban air quality [4], while also contributing to the reduction of greenhouse gas (GHG) emissions from the transport sector [5]. An electric vehicle is commonly defined as a vehicle powered by one or more electric motors for traction or propulsion [6].

Retrofitting refers to the process of replacing the existing ICE powertrain with an electric motor, battery pack, and associated components, thereby transforming a conventional vehicle into a zero-emission mode of transport. This approach not only extends the service life of existing vehicles but also provides a cost-effective solution to meet the increasing demand for electric mobility. Koengkan et al. [7] reported that battery-based electric vehicles are particularly effective in minimizing CO_2 emissions. Furthermore, the total cost of ownership is a critical factor influencing EV adoption. According to the European Consumer Organization, EV ownership offers cost savings and represents a more economical long-term solution compared to ICE vehicles powered by diesel or gasoline [8–11]. In countries such as India, where small commercial vehicles constitute the backbone of urban and semi-urban

goods transportation, retrofitting presents a highly practical pathway toward electrification. By converting existing ICE-based mini-trucks into electric vehicles, fleet operators and small business owners can transition to cleaner energy alternatives without incurring the high initial costs associated with purchasing new EVs.

The scope of ICE-to-EV retrofitting in India is expected to evolve with advancements in technology, regulatory developments, and market demand. The legality of such conversions depends on prevailing regulations and standards, which are subject to change; therefore, it is essential to remain updated on current laws governing EV conversions [12]. This study specifically considers the regulations and guidelines established by the Automotive Research Association of India (ARAI) that facilitate the retrofitting process. This work examines the technical, economic, and environmental aspects of converting ICE passenger cars to electric vehicles. It presents an analysis of the design modifications required for efficient conversion, addresses the technical hurdles and limitations, and explores the potential impacts on vehicle performance, safety, and sustainability. By providing a structured approach to ICE to EV conversions, this research seeks to support engineers, automotive enthusiasts, and policymakers in advancing the adoption of EV technology, maximizing existing resources, and contributing to a greener transportation ecosystem.

2. Literature Review

Recent studies have expanded the scope of electric vehicle (EV) retrofitting by incorporating computational analysis and broader perspectives on electric mobility adoption. Vashist et al,. [13] proposed a computational approach to evaluate vehicle suitability for EV retrofitment, aiming to accelerate the transition toward electric mobility. The study provides a systematic framework for identifying viable retrofit candidates; however, it focuses primarily on assessment methodologies and lacks detailed structural and component-level design validation. Similarly, Rahman and Thill [14] present a comprehensive review of factors influencing EV adoption within smart city contexts, highlighting challenges such as infrastructure, cost, and user acceptance. Although the study offers valuable insights into adoption trends, it does not specifically address the technical and mechanical aspects of retrofitting existing vehicles.

Gupta and Agarwal [15] provide a comprehensive review of retrofitting commercial vehicles, identifying key challenges such as system compatibility, battery integration, and structural modifications. While the study highlights environmental benefits, it remains largely conceptual without experimental validation. Hesse et al., [16] examine retrofitting potential in the German context using a mixed-methods approach, focusing on customer needs and business models. However, the findings are region-specific and may not be directly applicable to developing countries.

Studies focusing on the Indian context reveal additional constraints such as cost sensitivity, limited charging infrastructure, and evolving policy frameworks. Reports addressing EV retrofitting initiatives [17] discuss government targets and implementation challenges but lack detailed technical insights. In contrast, Sharma et al., [18] present a simulation-based and cost-oriented approach for ICE-to-EV conversion, offering practical insights into system design; however, the study is limited to specific vehicle configurations.

Policy-oriented studies such as [19] emphasize the environmental and economic advantages of retrofitting, particularly in reducing greenhouse gas emissions and extending vehicle life cycles. Nevertheless, they often overlook engineering design and real-world performance aspects. Technical investigations by Verma and Singh [20] and Reddy et al., [21] focus on component selection, integration challenges, and performance evaluation. These studies provide useful practical insights but are generally limited to small-scale applications such as passenger cars and two-wheelers.

Further, Studies demonstrate that retrofitting can play a significant role in accelerating the transition from fossil fuel–based vehicles by enhancing the affordability and accessibility of electric mobility; however, these analyses are predominantly policy-oriented and lack detailed engineering design and technical validation [22].

The existing literature demonstrates that EV retrofitting is a promising solution for sustainable transportation; however, significant gaps remain. There is a lack of integrated studies combining design, structural analysis, and performance evaluation for retrofitted systems, particularly for commercial vehicles under real operating

conditions. In addition, limited attention has been given to standardized design methodologies and component optimization. Therefore, the present work aims to address these gaps by focusing on the design, analysis, and validation of key components in an EV retrofitting system, ensuring both structural integrity and functional performance.

3. Methodology

The methodology begins with power calculations to estimate the required motor capacity based on vehicle performance requirements. This is followed by a detailed numerical analysis using MATLAB/Simulink to evaluate the dynamic behavior of the vehicle under various operating conditions. Based on these results, the design and modification of key EV components such as the motor mounting plate, clamp, coupler, and battery pack are carried out using AutoCAD (2023)**.** Subsequently, the modified designs are imported into ANSYS Workbench (2023 R2) for structural analysis and modal analysis to evaluate stress distribution, deformation, and overall structural integrity, ensuring safe and reliable operation

4. Conceptual Design

TATA 407 Gold SFC vehicle model has been selected as the reference platform for this study. The conceptual design of the electric vehicle retrofitting system illustrates the conversion of a conventional internal combustion engine (ICE) vehicle into an electric-powered vehicle by replacing key components with an electric drivetrain. The proposed design includes major components such as the electric motor, motor controller, DC-DC converter, battery pack, coupler, and charging port, integrated with the existing gearbox to ensure compatibility and functionality

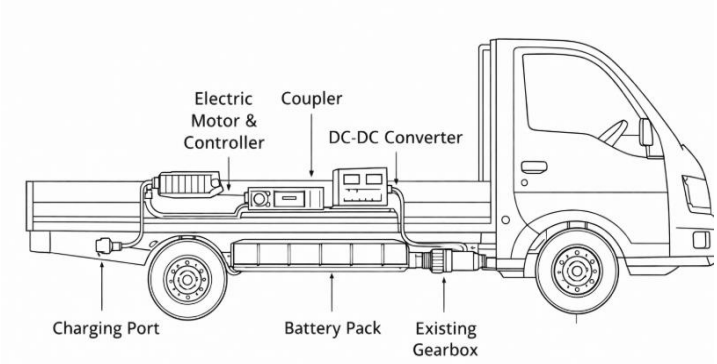

Fig.1 Conceptual layout of EV retrofitting system (CAD model)

5. V. Design Calculations

To design an efficient electric powertrain for the retrofitted vehicle, it is essential to estimate the motor power and torque requirements under various driving conditions. The total tractive effort required at the wheels is determined by considering the combined effect of inertial force, rolling resistance, aerodynamic drag, and gradient resistance. These forces are evaluated to ensure that the selected motor can meet performance requirements during acceleration, cruising, and hill climbing conditions. The total tractive force is given by:

$$R = F_I + F_f + F_d + F_g$$

where F_I is the inertia force, F_f is the rolling resistance, F_d is the aerodynamic drag, and F_g is the gradient resistance.

Based on these considerations, the motor power and torque are evaluated under the following driving scenarios:

1.Case 1: Acceleration in flat road 0 to 60 km/hr in 15s
2.Case 2: In constant speed in flat road 70 km/hr
3.Case 3: Acceleration in inclined road from 0 to 30kmph with θ= 15◦ in 15s

Motor torque and power needed under different driving conditions are

Case 1: Motor power on level Road

Inertia Force F_I= ma= 6937.5N
Frictional force $F_f=\mu_r$. mg = 735.75N
Drag force $F_d = 1/2\rho V^2 AC_d$ = 561N
Resistance $R_1 = F_I + F_f + F_d$ = 8234.25N
Torque on the wheel $T_1= R_1.r_w$ =3005.5NM
Power $P_1= R_1.V$ =137.265kW

Case 2: In constant speed in flat road

Inertia Force F_I = ma= 0, V = cont. (a =0)
Frictional force $F_f=\mu_r$ mg = 735.75N
Drag force $F_d = 1/2\rho V^2 AC_d$ = 762.6 N
Resistance $R_2 = F_f + F_d$ = 1498.35N
Torque on the wheel T = $R_2.r_w$=546.89 NM
Power $P_2= R_2.V$ =29.12kW

Case 3: Acceleration in inclined road from 0 to 30kmph with θ= 15°

Inertia Force F_I = ma= 3500N
Frictional force $F_f=\mu_r$. mg cosθ = 710.67N
Drag force $F_d = ½\rho V^2 AC_d$ = 140.03N
F_{in}= mg sinθ =15868.84N
Resistance $R_3 = F_I+F_f+ F_d+F_{in}$ = 20219.54N
Torque on the wheel $T_3 = R_3.r_w$ =7380N-m
Power $P_3= R_3.V$ =168.428 kw

6. Numerical Method

MATLAB/ simulink was utilized for drive cycle generation and subsequent torque and power calculations. A drive cycle represents a vehicle's speed profile over time under specific driving conditions, such as urban or highway environments. Using MATLAB/simulink, a custom drive cycle was generated that simulated real-world scenarios, providing essential data on speed, acceleration, and deceleration. This data was crucial for determining the torque demand and power requirements of the EV. Torque was calculated considering factors such as vehicle mass, wheel radius, and acceleration, while power was derived using the relationship between torque and angular velocity. The simulation model for EV powertrain is given in fig 2

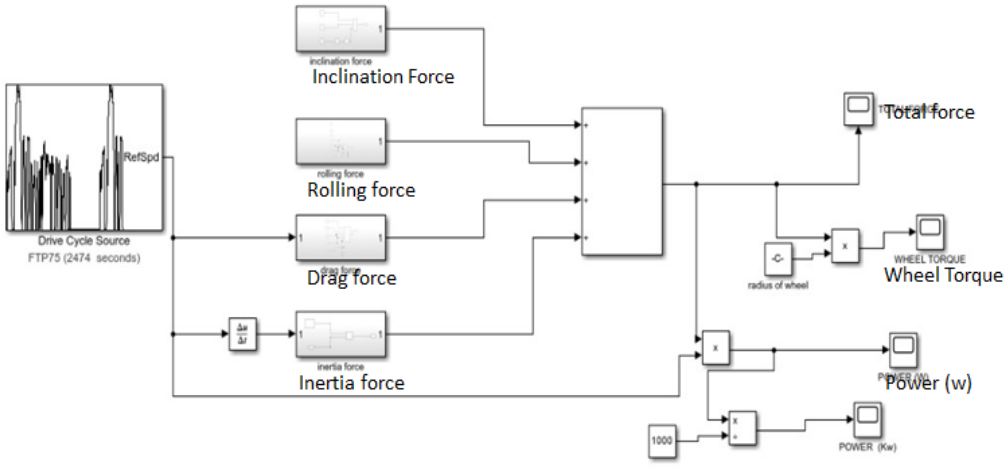

Fig. 2 Simulation model for EV power train

Numerical calculations for different drive cycles are g are given in table1and 2

Table 1: Mean power, Torque and Total force obtained from Simulink for vehicle on level road

Motor Power	142.54kW
Wheel Torque	4665.08 NM
Total Force	11052 N

Table 2: Motor power, Torque and Total force obtained from Simulink for vehicle on inclined road

Motor Power	83.60kW
Wheel Torque	6035.4 NM
Total Force	7346 N

7. Description of Major EV Components

A. Electric Motor

A PMSM motor with a power output ranging from 100 kW. Permanent Magnet Synchronous Motors (PMSMs) are advanced electric motors that utilize permanent magnets embedded within the rotor to produce a magnetic field. This unique design feature contributes to their exceptional performance characteristics. By harnessing the inherent magnetic properties of permanent magnets, PMSMs achieve higher power density and efficiency compared to other types of motors.

The use of permanent magnets allows for a more compact and streamlined motor design, resulting in a reduction in size without compromising performance. Moreover, PMSMs typically operate with efficiency levels ranging from 92% to 97%, making them highly desirable for energy-conscious applications. This high level of efficiency translates to lower energy consumption and reduced operating costs over the lifespan of the motor. The motor is mounted near the rear differential to simplify the drivetrain layout and reduce mechanical losses. Fig. 3 shows the model of PMSM motor.

Fig, 3 PMSM motor

B. Motor mounting clamp

The motor must be securely mounted to the chassis to prevent vibration, displacement, and shaft misalignment. Based on the mounting specifications of the Permanent Magnet Synchronous Motor (PMSM), a custom motor mounting system was designed to ensure optimal integration with the existing vehicle chassis. The motor is supported using a U-shaped bracket clamp welded to the vehicle chassis, providing strong support and vibration resistance. The dimensions of the motor mounting clamp are determined based on the geometry of the selected electric motor, load-bearing requirements, and structural stability considerations. The inner diameter (350 mm) of the clamp is selected based on the outer diameter of the electric motor housing. A small clearance is provided to allow easy assembly and to accommodate thermal expansion

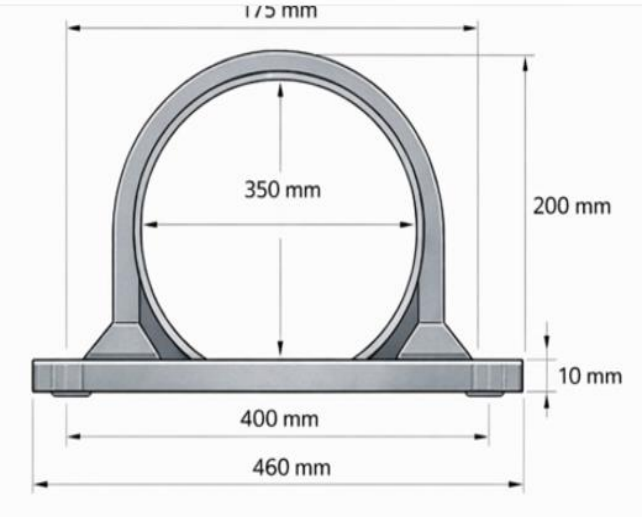

Fig .4 Motor Mounting Clamp

Clamp Material used is SAE 1045 steel. SAE 1045 is a medium-carbon steel with good strength, impact resistance, and toughness, making it suitable for engineering and industrial applications. Fig 4 shows the CAD model of the clamp.

C. Coupler

The coupler is a crucial component that ensures efficient torque transfer, mechanical stability, and proper alignment between the electric powertrain and the vehicle's drivetrain. The flexible jaw coupler is selected because it can accommodate minor shaft misalignment and reduce vibration and shock loads. The CAD model of the coupler is given as fig .5.

Fig.5 CAD model of coupler

The specifications of the coupler are determined based on the torque transmission requirements, shaft dimensions, and alignment conditions between the electric motor and the existing gearbox. The coupler diameter (60 mm) is selected based on the shaft diameter of the motor

D. Mounting plate

The motor mounting plate is a structural component that provides a rigid base for securing the electric motor to the vehicle chassis. It is typically fabricated from steel to ensure sufficient strength and stiffness to support the motor weight and withstand operational loads. The plate distributes the load from the motor evenly to the chassis, thereby preventing localized stress concentrations and improving the overall stability of the system. Fig 6 shows the CAD model of the mounting plate. The motor mounting plate is made of SAE 1045 steel, a medium carbon steel known for its good strength and durability.

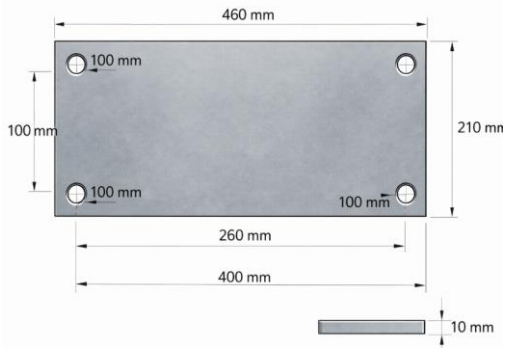

Fig. 6 Motor mounting plate

The dimensions of the motor mounting plate are determined based on load distribution, mounting requirements, and structural strength considerations. The overall length (460 mm) and width (210 mm) of the plate are selected to accommodate the footprint of the electric motor. The inner spacing (260 mm) represents the distance between mounting points, designed to match the bolt pattern of the motor base.

E. Battery

Lithium Iron Phosphate ($LiFePO_4$) is a type of lithium-ion battery that uses iron phosphate as the cathode material. It is widely used in electric vehicles due to its excellent safety, long lifespan, and stable performance under demanding operating conditions. Compared to other lithium-ion chemistries, $LiFePO_4$ batteries are less prone to overheating and thermal runaway, making them highly reliable for automotive applications. They provide a balanced combination of safety, durability, and cost-effectiveness. For commercial vehicles like mini-trucks, where reliability and long service life are critical. For a motor rated at 550 V, the battery pack nominal voltage should be 540–560 V (nominal), this ensures proper operation with some margin for voltage drop. Battery specifications are given in table 3 and battery pack model in fig,7.

Table 3: Battery Specifications ($LiFePO_4$)

Parameter	Value
Battery Type	Lithium Iron Phosphate
Nominal Cell Voltage	3.2 V
Cell Capacity	100 Ah
Motor Voltage Requirement	550 V
Pack Nominal Voltage	550.4 V
Total Energy Required	165 kWh
Final Configuration	172S × 3P
Total Cells	516 cells
Pack Capacity	300 Ah

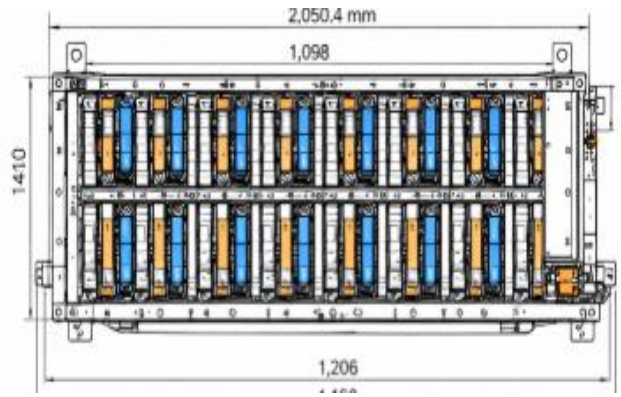

Fig. 7 Battery pack model

F. EV Controller

The electric vehicle controller is an electronic unit positioned between the battery pack and the motor, responsible for regulating the vehicle's speed and acceleration. It manages the flow of energy by converting the battery's direct current (DC) into alternating current (AC) required for motor operation. Additionally, the controller enables both manual and automated control of motor start and stop functions, facilitates forward and reverse motion, and provides protection against overloads and electrical faults.

8. Static Analysis

Static analysis of EV components refers to the evaluation of structural behavior under steady or non-varying loads to ensure mechanical integrity and safety. It is commonly performed using Finite Element Analysis (FEA) to determine parameters such as stress distribution, deformation, and strain in components like motor mounting plate, clamp and coupler. This analysis helps identify critical stress regions, verify that stresses remain within material limits, and optimize the design for durability and reliability under real operating conditions.

9. Modal Analysis

Modal analysis (Dynamic) is performed on the machine components to study its natural frequencies and mode shapes, ensuring that it does not resonate with the operating frequencies of the motor. This is crucial to prevent excessive vibrations, which could lead to fatigue failure and structural instability.

10. Results and Discussion

Analytical and numerical approaches were employed to evaluate the vehicle's power, wheel torque, and total resistance forces, including rolling resistance, aerodynamic drag, and gradient force. While analytical calculations were based on standard vehicle dynamics equations, a MATLAB/Simulink model was developed to simulate real-world driving conditions and obtain corresponding performance parameters.A comparison of the results indicates that the numerical method predicts slightly higher power and torque values, primarily due to its ability to capture transient effects and system non-linearities. Although the torque values obtained exceed the direct motor output, this is justified by drivetrain elements such as gear reduction and differential mechanisms, which amplify the torque at the wheels.

Based on the design calculations carried out using both analytical and numerical methods, a PMSM motor was selected for the EV truck. The corresponding motor specifications are presented in Table 4.

Table 4: Motor Specifications

Parameter	Value
Rated Power	100 kW
Peak Power	120 kW
Rated Voltage	550 V
Rated Speed	3000 rpm
Maximum Speed	4000 rpm
Peak Torque	1200 Nm
Efficiency	94 – 96 %
Motor Diameter	340 mm
Motor Length	320 mm
Motor Weight	150 kg
Cooling Method	Liquid Cooling
Reduction Gear	3 – 4 :1

The mechanical components, including the motor mounting plate, coupler, and clamp, were subjected to both static and dynamic analyses.

A. Static Analysis of Motor Mounting Plate

The static analysis results(fig.8) indicate extremely low levels of strain, stress, and deformation in the component. The maximum equivalent strain (4.77×10^{-7} mm/mm) and maximum principal strain (1.30×10^{-7} mm/mm) are uniformly distributed, with slight concentrations near bolt holes and edges.

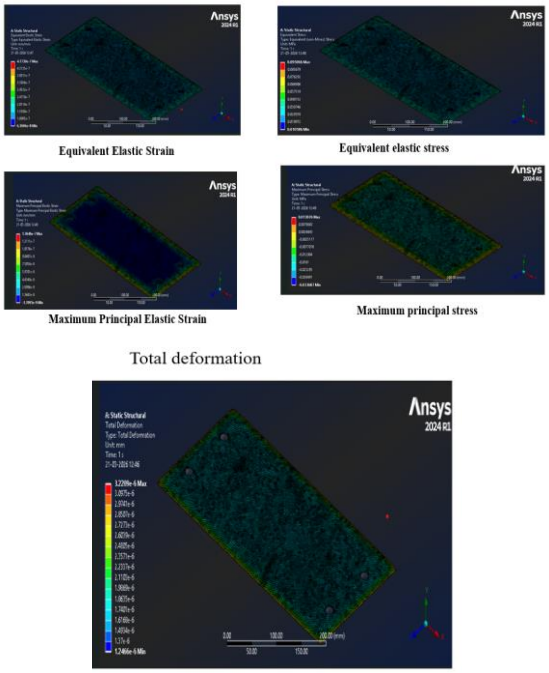

Fig.8 static analysis result of motor mounting plate

The maximum stress obtained (0.095 MPa) is significantly lower than the yield strength of SAE 1045 steel (310 MPa), confirming safe operation within the elastic limit. Additionally, the deformation is negligible (3.22×10^{-6} mm), with maximum displacement at the central region and minimal deflection near constrained areas, indicating high structural stiffness and integrity.

B. Static Analysis of Coupler

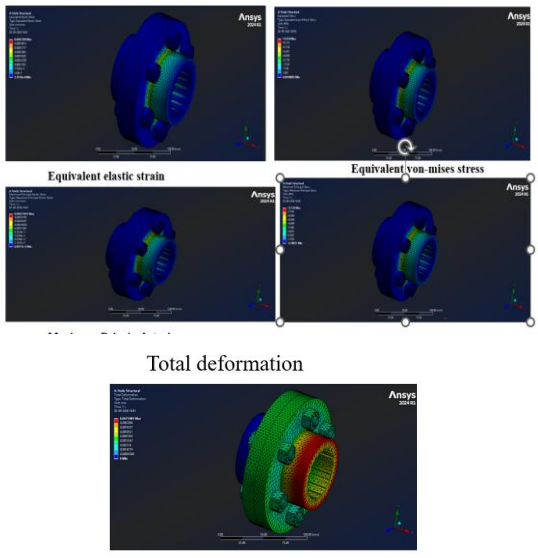

Fig. 9 static analysis result of coupler

The analysis (fig.9) shows that the maximum strain (0.0003309 mm/mm) and maximum principal strain (0.00021043 mm/mm) are concentrated at the shaft–hub and hub–jaw interface regions, respectively, while the remaining areas exhibit negligible strain. The maximum stress (53.45 MPa) and principal stress (31.139 MPa) are also localized at these contact regions, with minor compressive stress (−0.788 MPa) observed, whereas most of the component experiences low stress levels. The maximum deformation is 0.0075481 mm, occurring at the outer hub and spline region, with minimal displacement at fixed regions, indicating that the coupler is safe, stable, and reliable for operation**,** with only the interface region requiring consideration for fatigue under cyclic loading.

C. C.Static Analysis of Clamp

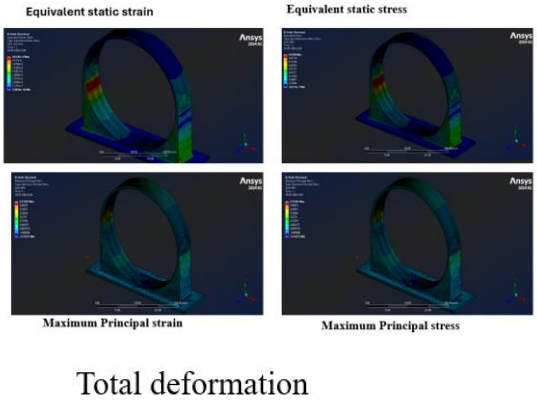

Fig. 10 static analysis result of clamp

The results (fig.10) indicate that the maximum strain (4.65×10^{-6}) and principal strain (2.46×10^{-6}) are concentrated at the inner curved junction between the ring and the base, identifying it as the critical deformation region, while the rest of the structure exhibits low strain and good stiffness. The maximum stress (0.93 MPa) and tensile stress (0.54 MPa) are also localized at this junction, with minor compressive stress (−0.14 MPa) present in some regions, indicating overall stable stress distribution. The maximum deformation (0.000582 m) occurs at the loaded upper region, gradually decreasing toward the fixed base, confirming bending behavior with minimal displacement at constrained regions. The loading conditions and constraints of overall static analysis are given in table 5.

Table 5: Static Analysis – Loading and Boundary Conditions

Component	Load Type	Load Magnitude	Loading Nature	Constraints
Motor Mounting Plate	Motor weight (vertical force)	981 N	Static	Bolt holes fixed to chassis
Motor Clamp	Design load (with FOS = 3)	4413 N	Static	Base fixed; load on curved surface
Coupler	Torque transmission	1272 Nm	Static (torsional)	One end fixed; torque at shaft–hub

D. Dynamic analysis of mounting plate

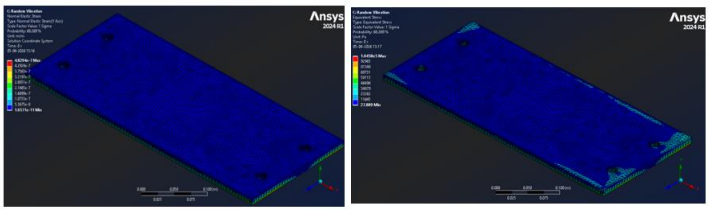

Normal strain Equivalent stress

Fig. 11 Dynamic analysis of mounting plate

The contour plots in fig.11 indicate predominantly low strain and stress across the structure, with most regions exhibiting minimal values. However, localized concentrations are observed near edges, corners, and mounting holes due to geometric discontinuities and boundary constraints. These regions represent critical points that are more susceptible to deformation and stress intensification under random vibrational loading

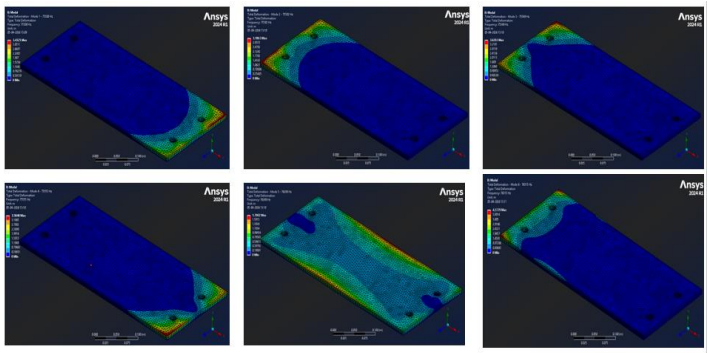

Fig.12Total deformation at different vibrational frequencies

The first two modes exhibit closely spaced natural frequencies, indicating the possibility of modal coupling, with deformation primarily localized near the edges and less constrained regions.

The next 3 Modes the deformation patterns become progressively more complex, shifting between different regions and spreading across the plate, representing higher-order bending and twisting effects. In last Mode the maximum deformation is concentrated near corners and around hole regions, highlighting these areas as structurally weaker and more susceptible to vibration. The reults are given in fig.12.

The analysis shows that deformation is largely influenced by geometry and boundary conditions, with critical stress-prone zones occurring near edges and discontinuities, which may require reinforcement for improved structural performance and durability.

E. Dynamic analysis of the Coupler

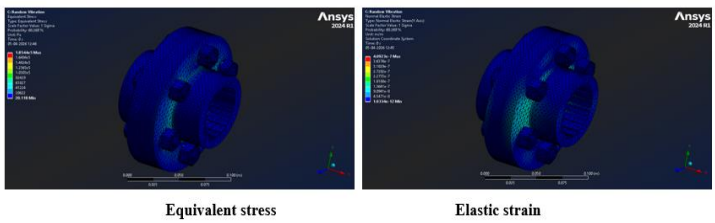

Equivalent stress Elastic strain

Fig .13 Dynamic analysis of the coupler

The results (fig,13) indicate that the maximum stress (0.185 MPa) and strain (4.09×10^{-7} mm/mm) are concentrated at the shaft–hub interface and jaw regions, while the remaining areas exhibit negligible values. This suggests that these regions are more susceptible to vibrational loading and experience relatively higher deformation due to dynamic force transmission.

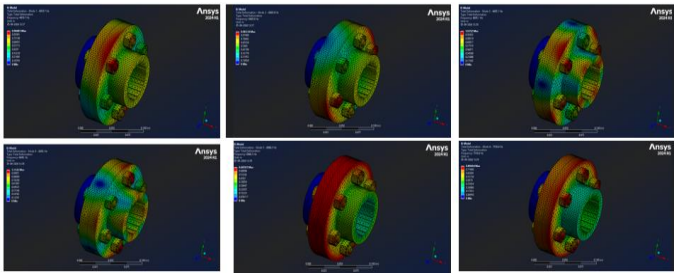

Fig. 14 Total deformations

The result (fig.14) shows the total deformation distribution of the coupler under loading conditions. The maximum deformation occurs at the outer hub and jaw region, (red and yellow zones), the minimum deformation is observed at the constrained or fixed regions (blue zone).

The deformation gradually decreases from the load application area towards the opposite end, indicating a smooth and uniform displacement pattern. At the three high-order modes, the results reveal a transition from complex torsional-bending to more localized transverse bending and rocking motions The maximum displacement remains concentrated on the outer periphery of the flange(red). The splined hub maintains structural stability as indicated by the minimal deformation (blue) regions. Design of the coupler considered is safe and capable of withstanding the applied loads without significant distortion

F. Dynamic analysis of clamp

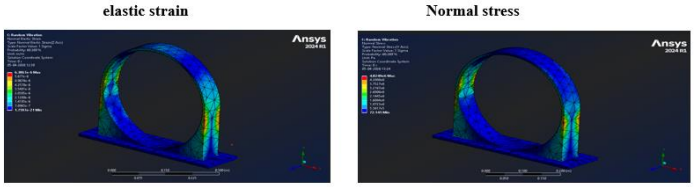

Fig.15 Dynamic analysis of the clamp

The results indicate that the maximum strain (6.39×10^{-6}) and stress (4.82 MPa) are concentrated at the curved junction and vertical support regions of the ring, while the base experiences minimal values due to constraints. The smooth distribution of stress and low strain magnitude confirm effective load transfer, adequate strength, and good dynamic stability under random vibration conditions. The results are given in fig. 15.

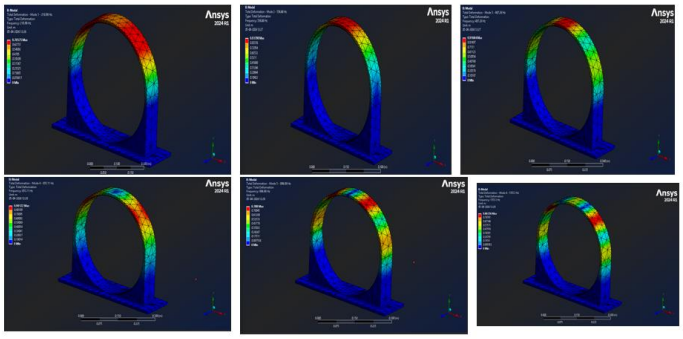

Fig.16 Total deformations at different vibrational frequencies

The total deformation results obtained from ANSYS indicate that the structure experiences maximum displacement at the upper curved region of the ring

The different modes obtained from different vibrational frequencies ranging from 200 to 1335 Hz are shown in fig.16. Higher modes exhibit more complex deformation shapes with multiple peaks. In general magnitude of deformation remains relatively low, confirming that the structure possesses adequate stiffness and maintains stable performance under and dynamic loading conditions. The loading conditions and constrains are given in table 6.

Table 6: Dynamic Analysis – Loading and Boundary Conditions

Component	Excitation / Load	Loading Nature	Boundary Conditions
Motor Clamp	Strain:6.39×10^{-6}	Stochastic vibration	Base fixed; curved Region active
Motor Clamp	218 – 1355 Hz	Free vibration	Base fixed; rest free
Coupler	Stress 0.185 MPa	Dynamic torsional vibration	Hub constrained
Coupler	6698 – 7556 Hz	Free vibration	Hub fixed; flange free
Mounting Plate	Stress 1.05×10^{5} Pa	Stochastic vibration	Bolt holes fixed
Mounting Plate	75 – 76 kHz	Free vibration	Bolt holes fixed

11. Conclusion

This study establishes the technical feasibility of retrofitting an internal combustion engine mini truck into an electric vehicle through integrated analytical modelling and MATLAB/Simulink-based simulation. The analytical results indicated a motor torque requirement of approximately 1272 Nm and a wheel torque of 7380 Nm with a gear ratio of 5.8:1. The mounting load was calculated as 1471 N, with a design load of 4413 N (FOS = 3), and the shaft diameter was determined as 55 mm. MATLAB-based drive cycle analysis provided realistic vehicle performance data, leading to the selection of a 100 kW PMSM motor and a suitable battery system, thereby validating the drivetrain configuration.

Finite Element Analysis (FEA) using ANSYS confirmed the structural integrity of key components. The mounting plate exhibited a maximum stress of 0.095 MPa, deformation of 3.22×10^{-6} mm, and a high factor of safety of approximately 3263. The clamp showed a maximum stress of 0.93 MPa and deformation of 0.000582 m, while the coupler experienced a maximum von Mises stress of 53.45 MPa and deformation of 0.0075 mm. In all cases, stress and strain values were significantly below material limits, confirming safe operation under static loading conditions. The developed CAD models of the mounting plate, clamp, and coupler further ensured design feasibility and manufacturability.

Dynamic analysis demonstrated that the system possesses adequate stiffness and stability under vibrational conditions. Random vibration results showed very low stress (maximum ≈ 0.185 MPa) and negligible strain levels (10^{-6} to 10^{-7} range). Modal analysis revealed natural frequencies of 218–1355 Hz (clamp), 6698–7556 Hz (coupler), and 75–76 kHz (mounting plate), which are well above operational excitation ranges, thereby eliminating resonance risks. Overall, the results confirm that the proposed retrofit system is structurally robust, dynamically stable, and functionally viable, highlighting its potential as a sustainable solution for converting conventional mini trucks into energy-efficient electric vehicles.

References

[1] S. Vasanthaseelan, D. S. Dharun, S. Sreerag, and R. Gokul, "Conversion of IC engine vehicle to electric vehicle," *Int. Res. J. Eng. Technol. (IRJET)*, vol. 6, no. 3, 2019.

[2] S. Bhattacharjya, T. Kaushik, A. Pandey, and M. Singh, *Comparative analysis of electric vehicles and internal combustion engine vehicles from resource efficiency perspective*, New Delhi, India: The Energy and Resources Institute (TERI), Jul. 2023.

[3] D. M. Karthik and A. C. Giriyapur, "Retrofitting of an engine powered vehicle into an electric vehicle," in *Proc. 2nd Int. Conf. Smart Syst. Inventive Technol. (ICSSIT)*, 2019, ISBN: 978-1-7281-2119-2

[4] C.-M. Lai, Y.-H. Chang, M.-H. Hsieh, and Y.-C. Lin, "Development of a bidirectional DC/DC converter with dual-battery energy storage for hybrid electric vehicle system," *IEEE Trans. Veh. Technol.*, vol. 67, no. 23, 2018.

[5] A. Karki, S. Phuyal, D. Tuladhar, S. Basnet, and B. P. Shrestha, "Status of pure electric vehicle power train technology and future prospects," *Appl. Syst. Innov.*, vol. 3, no. 35, 2020. http://www.electricvehiclesnews.com.

[6] M. Koengkan, J. A. Fuinhas, M. Teixeira, E. Kazemzadeh, A. Auza, and F. Dehdar, "The capacity of battery-electric and plug-in hybrid electric vehicles to mitigate CO_2 emissions: Macroeconomic evidence from European Union countries," *World Electr. Veh. J.*, vol. 13, no. 4, p. 58, 2022.

[7] M. Dotoli, R. Rocca, M. Giuliano, G. Nicol, F. Parussa, M. Baricco, A. M. Ferrari, C. Nervi, and M. F. Sgroi, "A review of mechanical and chemical sensors for automotive Li-ion battery systems," *Sensors*, vol. 22, p. 1763, 2022, doi: 10.3390/S22051763.

[8] Z. A. Lashari, J. Ko, S. Jung, and S. Choi, "Choices of potential car buyers regarding alternative fuel vehicles in South Korea: A discrete choice modeling approach," *Sustainability*, vol. 14, p. 5360, 2022, doi: 10.3390/su14095360.
[9] K. A. Mamun, F. R. Islam, R. Haque, A. A. Chand, K. A. Prasad, K. K. Goundar, K. Prakash, and S. Maharaj, "Systematic modeling and analysis of on-board vehicle integrated novel hybrid renewable energy system with storage for electric vehicles," *Sustainability*, vol. 14, p. 2538, 2022, doi: 10.3390/su14052538.
[10] F. H. Gandoman, E. M. Ahmed, Z. M. Ali, M. Berecibar, A. F. Zobaa, S. H. E. A. Aleem, and E. M. Ali, "Reliability evaluation of lithium-ion batteries for e-mobility applications from practical and technical perspectives: A case study," *Sustainability*, vol. 13, p. 11688, 2021, doi: 10.3390/su132111688.
[11] R. S. Patel and A. Mishra, "Scope of retrofitting ICE vehicle into electric vehicle in India," *Int. J. Sci. Eng. Technol.*, vol. 11, no. 5, 2023.
[12] D. Vashist, M. Jain, and J. Jain, "Computational analysis for vehicle suitability for EV retrofitment: An approach for faster transition to electric mobility," *SAE Tech. Paper* 2025-28-0400, Oct. 2025.
[13] M. Rahman and J.-C. Thill, "A comprehensive survey of the key determinants of electric vehicle adoption: Challenges and opportunities in the smart city context," *World Electr. Veh. J.*, vol. 15, no. 12, p. 588, Dec. 2024.
[14] P. Gupta and S. Agarwal, "Review on retrofitting of commercial vehicles from IC engines to electric powertrains," *Int. J. Veh. Des.*, 2021.
[15] H. H. Hesse, A. Müller, and M. Wietschel, "Internal combustion engine to electric vehicle retrofitting: Potential, customer needs, public perception, and business model implications," *Transp. Res. Interdiscip. Perspect.*, vol. 10, p. 100386, 2021, doi: 10.1016/j.trip.2021.100386.
[16] SAE International, "Insights into retrofitting internal combustion engine vehicles to electric vehicles," *SAE Tech. Paper Series*, n.d. [Online]. Available: https://www.sae.org/
[17] S. Sharma, R. Kumar, and A. Singh, "Experimental electric retrofitting of an ICE vehicle with simulation and cost analysis," *Int. J. Eng. Res. Technol.*, vol. 13, no. 3, pp. 45–52, 2024.
[18] Global Green Growth Institute, *Electric vehicle retrofitting: A guide to policy-making*. 2020. [Online]. Available: https://www.greenpolicyplatform.org
[19] A. Verma and P. Singh, "Retrofitting of an engine powered vehicle into an electric vehicle," *Int. J. Sci. Eng. Res.*, vol. 10, no. 6, pp. 123–129, 2019. [Online]. Available: https://www.ijser.org
[20] K. Reddy, S. Kumar, and M. Rao, "Retrofitting of IC engine bike into geared electric bike," *Int. J. Res. Eng. IT Soc. Sci.*, vol. 12, no. 1, pp. 67–74, 2024. [Online]. Available: http://www.indusedu.org
[21] Transport & Environment, "Ending the ICE age – Can e-retrofit help Europe phase out fossil fuel cars?" 2021. [Online]. Available: https://www.transportenvironment.org